



Full Text View

Volume 30, Issue 5 (May 2000)

Journal of Physical Oceanography

Article: pp. 987–1012 | [Abstract](#) | [PDF \(2.72M\)](#)

Interannual Dynamics and Thermodynamics of the Indo–Pacific Oceans

A. Schiller, J. S. Godfrey, P. C. McIntosh, G. Meyers, and R. Fiedler

CSIRO Division of Marine Research, Hobart, Tasmania, Australia

(Manuscript received June 12, 1998, in final form May 24, 1999)

DOI: 10.1175/1520-0485(2000)030<0987:IDATOT>2.0.CO;2

ABSTRACT

A global ocean circulation model, driven by observed interannual fluxes, is used to gain insight into how sea surface temperature anomalies (SSTAs, i.e., variations from the mean seasonal signal) in the tropical and subtropical Indian and Pacific Ocean are maintained and changed on interannual timescales. This is done by investigation of heat in the upper ocean at five selected sites and by comparison to observations based on expendable bathythermograph data and the TOGA/TAO moored buoys. A 6-yr simulation between 1985 and 1990 reveals that the model's simulated interannual temperature variability in the upper 450 m of the ocean is in reasonable agreement with observations. However, the model overestimates the meridional extent and amplitude of SST variability in parts of the equatorial Pacific and Indian Oceans. The problem is associated with the choice of heat flux boundary condition: the ratio of air humidity to saturated humidity over freshwater at SST in the latent heat flux term is independent of the spatial scale of SSTA pattern, which implies a weaker negative feedback on SST change.

In the central Pacific at (0°, 140°W), budgets for the surface mixed layer and over the top 300 m both show the primary causes of temperature change to be zonal and vertical advection, with their sum generally less than half of either term individually. At (0°, 110°W), the mixed layer is much thinner so that the temperature changes result from a small disturbance of a basic balance between the vertical convergence of heat flux and vertical and zonal advection. At both sites the zonal flow (and hence the zonal heat advection) is determined by a sum of several terms, none of which are small. It is therefore difficult to find a clear physical basis in the model for the Kessler–McPhaden empirical rule for SSTAs, which correlates highly with observed SSTAs. However, this rule suggests that differences between wind stress products that exceed 0.04 N m^{-2} over several months (as occurs at 140°W in 1989) could lead to differences in SSTAs of up to 4°C. This may help explain the occurrence of a short but intense La Niña episode that occurred in the model, but not in the observed SST. Comparison with earlier model results tends to confirm that FSU winds were in error in the east Pacific in late 1989 and suggests that the use of a realistic (thin) surface mixed layer exacerbates the problem by strengthening the sensitivity of SSTAs to wind errors.

A simple time integral of the depth-averaged (0–350 m) current at 140°E, near the western boundary of the equatorial Pacific, shows a clear correlation with the zonal movements of the eastern edge of the warm pool, lagged by about six months. This is qualitatively as expected from “delayed oscillator” theory and confirms that the basic current structure of our model is in close agreement with observations.

Table of Contents:

- [Introduction](#)
- [Overview: Simulated and Low-latitude interannual Summary and discussion](#)
- [REFERENCES](#)
- [TABLES](#)
- [FIGURES](#)

Options:

- [Create Reference](#)
- [Email this Article](#)
- [Add to MyArchive](#)
- [Search AMS Glossary](#)

Search CrossRef for:

- [Articles Citing This Article](#)

Search Google Scholar for:

- [A. Schiller](#)
- [J. S. Godfrey](#)
- [P. C. McIntosh](#)
- [G. Meyers](#)
- [R. Fiedler](#)

Model and XBT observations show strong similarities in the depth of the 20°C isotherm and SSTA along the IX1 section from western Australia to Java during 1985–90. SST close to the southern end of this section (23°S, 112°E) is dominated by the annual signal with a superimposed weak interannual signal. The time rate of change of accumulated temperature anomalies in the top 450 m is dominated by anomalous cold vertical advection from late 1986 to early 1988 with the opposite happening from late 1988 to early 1990. Both signals indicate the arrival of the ENSO signal along the northwest Australian coast with a reduced (increased) thermocline thickness during the El Niño (La Niña) event. SSTA at 23°S, 112°E in the model is controlled by a balance between anomalous vertical advection and total diffusion; SSTA is not driven by local heat fluxes.

1. Introduction

Sea surface temperature (SST) largely governs the exchange of energy between ocean and atmosphere; therefore an ocean model used for climate variability studies must have a reasonable simulation of SST. In particular, interannual variations of SST in the lower latitudes are of crucial importance to such climatic phenomena as El Niño–Southern Oscillation (ENSO), which is why modeling them has become a focus of international research over the last decade. The Tropical Ocean Global Atmosphere (TOGA) Program (WMO 1995a), for example, combined modeling with collecting high-quality hydrographic and meteorological data in the tropical Pacific Ocean. By understanding the tropical oceans and global atmosphere, the program aimed to understand El Niño, with the ultimate goal of improving predictions. However, as there are many processes involved in the tropical coupled ocean–atmosphere system, some aspects of ocean general circulation models (OGCMs) are still poorly understood and need further investigation. An example is the cold bias along the equator in the eastern Pacific Ocean, which is found in most numerical simulations (e.g., Stockdale et al. 1993). Furthermore, even recently increased efforts to collect data in the Indonesian Throughflow (ITF) region have not provided a sufficiently accurate time series in this climatically important area [see Godfrey (1996) for a review], making any assessment of model simulations in the ITF difficult.

It has been widely accepted that tropical oceans and atmosphere behave as a coupled system with large variability at the interannual timescale. The origin of this timescale has been traced to low-frequency changes in the upper ocean, particularly the tropical Pacific Ocean (Trenberth 1996). As the impact of climate variability on the economic, social, and natural environment increases (WMO 1995b) better predictions and understanding of low-latitude physics become more urgent. As part of an Australian Community Ocean Modelling effort, we are trying to improve the simulation and understanding of the processes in the Indo–Pacific oceans that influence low-latitude climate variability. Apart from the dominating ENSO signal in the Pacific Ocean, there is observational evidence that parts of the Indian Ocean (e.g., Leeuwin Current) are also affected on seasonal-to-interannual timescales by ENSO (Clarke and Liu 1994; Meyers 1996; Molcard et al. 1996). Empirical research has indicated that Indian Ocean SSTs are related to rainfall anomalies in parts of Australia (Nicholls 1989; Drosowsky 1993), which appear to be related to ENSO (Nicholls 1996). Part of this paper is devoted to the Indian Ocean to identify which interannual signals are correlated with ENSO.

In a previous paper (Schiller et al. 1998, paper I hereafter) we compared the surface heat flux our model needs to simulate the observed seasonal SST with observed heat fluxes and we compared the seasonal evolution of the mixed layer and steric height with observations in the Indian Ocean. The impact of simulated Indonesian tidal mixing on heat fluxes and water properties, and the structure of the Indonesian Throughflow were compared with observations.

Here we use an identical model configuration, but with interannual forcing in both the Pacific and Indian Oceans, as follows. Within 30° of the equator interannually varying estimates of monthly mean “pseudo wind stress” from the Florida State University (FSU; Legler et al. 1989; Stricherz et al. 1992) are applied. Poleward of 30°, the data have been blended into the Helleman and Rosenstein (1983) seasonal mean wind stresses. The heat fluxes are parameterized following Seager et al. (1988) and Chen et al. (1994a), with the International Satellite Cloud Climatology Project (ISCCP) “bulk” estimate of monthly mean net downward shortwave radiation (Li 1995). The shortwave radiation product is limited to the period 1985–90, which determined the integration period. The interannual experiments are based on a 20-yr spin up from rest with a mean seasonal forcing based on an average of the interannual forcing fields. Table 1 shows details of the model configuration, surface forcing fields, and experiment.

In this paper, we examine the model’s interannual variability, especially that of SST, in both Pacific and Indian Oceans. We want not only to document any success in generating observed SST anomaly (SSTA) patterns; we also want to assess whether state-of-the-art OGCMs can provide an adequate understanding and improve predictability of interannual variability in the Indo–Pacific basin.

At present, this kind of work is a severe test on any OGCM, for two reasons. First, outside the eastern tropical Pacific, SSTAs are relatively small and shortlived. Second, the presently available, interannually varying heat flux products are probably not adequate for simulating such SSTAs. In practice, present OGCMs forced by flux products do not simulate SSTAs very well. This paper is a first step toward solving the twin problems of improving ocean model physics and the fluxes that drive them (WMO 1996).

Section 2 gives an overview of simulated and observed SSTAs between 1985 and 1990. Section 3 validates the model results with observations from XBT and buoy data in the Pacific and Indian Ocean. The role of the Indonesian Throughflow in forming SSTAs in the Indian Ocean is investigated. Section 4 summarizes the results; it includes a discussion of problems

2. Overview: Simulated and observed interannual variability of the upper Indo–Pacific oceans

One measure of the performance of our ocean model is given in [Fig. 1](#). The observed SSTAs ([Reynolds 1988](#); [Reynolds and Smith 1994](#)), hereafter Reynolds SST, were correlated with the respective model values between 1985 and 1990. The model clearly works best over the central Pacific and at latitudes around 20°N and S toward the American continent (correlation >0.6, locally exceeding 0.8). It is moderately good in the Indian Ocean, with a few patches in the Indo–Pacific area showing small or even negative correlations.

The simulated interannual SST variability over most parts of the Indo–Pacific oceans is comparable in magnitude to observations ([Fig. 2](#)). The model overestimates the meridional extent of the SSTAs in the Pacific and also the amplitude of SSTAs in the western Indian Ocean, in the central and particularly in the eastern Pacific. The reason the model gets SSTAs that are too large may lie in our choice of heat flux boundary condition. Essentially, as in [Seager et al. \(1988\)](#) and [Chen et al. \(1994a\)](#), we represent latent heat loss by $\rho_a C_E L_{\text{W}} W q_{\text{sat}}(\text{SST}) \times (0.98 - \delta)$, where δ —the ratio of air humidity to saturated humidity over freshwater at SST—is taken from climatology [ρ_a , C_E , and L_{W} are, respectively, air density, bulk transfer coefficient, and latent heat of vaporization; W is wind speed; and $q_{\text{sat}}(\text{SST})$ is the saturated water vapor pressure over freshwater at SST]. Since δ is typically about 0.75, this implies a rather small sensitivity of latent heat loss to changes in SST. Models such as [Kleeman and Power \(1995\)](#) and [Seager et al. \(1995\)](#) allow for the dependence of δ on the spatial scale of the SST pattern over which the wind blows, which on average increases the sensitivity of latent heat loss to SST. Since greater sensitivity implies a stronger negative feedback on SST change, SST anomalies are expected to be smaller with a scale-dependent heat flux formulation. This may also explain why the modeled equatorial Pacific SSTA pattern is wider than the observed ([Fig. 2](#)); if the negative feedback on SSTA is too weak, water upwelled along the equator with an anomalous temperature will be advected too far poleward by Ekman transports before equilibrating with the atmosphere above it (e.g., [Seager et al. 1988](#)). A similar tendency for equatorial SSTAs to be too strong is also seen in [Brady \(1994\)](#) who, like us, used the [Seager et al. \(1988\)](#) surface heat flux condition.

To gain a more detailed view of the dominant interannual variations, the principal empirical orthogonal function (EOF) of the model’s SSTA together with the associated component time series was computed and compared with Reynolds’ observed SSTA ([Reynolds 1988](#); [Reynolds and Smith 1994](#)). The leading EOFs of the modeled and observed SSTAs are shown in [Fig. 3](#), together with the component time series. Not surprisingly, the dominant signal is related to ENSO and is located in the central and eastern Pacific. In contrast, the Indian Ocean reveals only small amplitudes. The first EOF of the model ([Fig. 3a](#)) shows good agreement with the observations ([Fig. 3b](#)), although the ENSO signal in the observations is more confined to the equator and has a larger amplitude there. The explained variances for modeled (52.4%) and observed (54.6%) SSTAs are very similar. The temporal components of the SSTAs ([Fig. 3c](#)) reveal two ENSO events during the integration period (i.e., warm event during 1986/87 and cold event during 1988/89). Both temporal curves depict some conformity (correlation = 0.6); though there are large deviations during the first and last year of integration. The deviations during the first year may simply reflect that the model has been driven only with mean seasonal forcing prior to 1985.

An EOF analysis for the upper-ocean heat content anomalies relative to 450 m was made on the subsurface structure of interannual variations. The structure of the leading EOF of heat content anomaly in the Pacific ([Fig. 4a](#)) is consistent with the corresponding ENSO pattern of SSTAs shown in [Fig. 3a](#). The corresponding time series ([Fig. 4b](#)) is much more similar to the observed SSTA time series—that is, to the Southern Oscillation index (SOI, not shown)—than the model SSTA of [Fig. 3c](#). Furthermore, the leading EOF of heat content anomalies shows a pronounced signal that extends from the Pacific into the Indian Ocean, with the largest amplitudes along the Australian coast, consistent with the analyses of [Meyers \(1996\)](#). The first EOF of heat content anomaly ([Fig. 4](#)) is quite similar to that shown by [Hirst and Godfrey \(1994\)](#) 9–18 months after the opening of the Indonesian Throughflow in their model (their [Figs. 2](#) and [12](#)).

We also investigated joint EOFs of SST and heat content. The resulting spatial and temporal structures produced very similar results and captured very similar variances to those from the individual analysis, indicating a coherent signal in SST and heat content.

3. Low-latitude interannual variability in the Indo–Pacific oceans

[Figure 5](#) shows a pair of Hovmoeller plots of SSTAs for the model and Reynolds data, respectively, along the equator, in both oceans. Both plots are dominated by the 1986–87 El Niño and the 1988–89 La Niña events, and display obvious spatial coherence over large zonal distances. For example, SSTAs for the whole Indian Ocean sector are quite coherent on the equator; model and Reynolds data are fairly similar. Therefore, one only needs to look at representative longitudes to characterize them, for example, the crossing of XBT lines. These longitudes, shown as vertical dashed lines in [Fig. 5](#) as well as in a geographical site map ([Fig. 6](#)), will be discussed in [sections 3a–c](#).

In the Pacific sector, we note a problem in the model with the timescales of both the 1985–87 extended warm period and the 1989–90 extended cold period. While the early warm phase could result from switching the forcing from varying seasonally to interannually, this does not explain the extended cold period. Only two previous studies appear to have examined Pacific SST in an OGCM driven by observed, interannually varying winds. The first ([Davey et al. 1994](#)) used a Bryan–Cox model quite similar to ours, but with a simpler surface heat flux boundary condition. The second ([Brady 1994](#)) used [Gent and Cane’s \(1989\)](#) model in which the mixed layer depth was held constant at 50 m. Both models were driven by FSU winds. Both (particularly [Davey et al. 1994](#)) obtained SSTA patterns in 1989–90 that were qualitatively very similar to

our simulation near 100°W in mid-1989, but they were weaker than those obtained by [Brady \(1994\)](#) and ourselves. All three simulations produce strongly positive anomalies in early 1990. In contrast, observed SSTAs remained positive throughout this period, but weakly decayed. Below we attempt to find whether this problem is due to deficiencies in the model's physics, or to errors in wind forcing. We picked two spots for comparison with the Tropical Ocean Global Atmosphere/Tropical Atmosphere–Ocean (TOGA/TAO) array: the central (0°, 140°W) and east (0°, 110°W) Pacific.

In addition to these sites, we compare model results with XBT data in the Indonesian archipelago where strong tidal mixing modifies the water mass structure and SST ([Ffield and Gordon 1996](#)). Furthermore, we investigate ocean dynamics along the IX1 XBT line (Fremantle–Java), which intersects the ITF. Finally, we chose a site in the equatorial Indian Ocean, where the semiannual Wyrтки jet is expected to modify SSTA.

The following Sections examine the (3a) Pacific Ocean, (3b) ITF, and (3c) Indian Ocean. In each section we compare anomalies of potential temperature against time and depth, from the model with TOGA/TAO or XBTs, depending on location. Model data and TOGA/TAO data are monthly averages, whereas the XBT data for the Indian Ocean and ITF are 2-month moving averages. (For a detailed discussion of potential biases caused by comparing datasets averaged over different times see paper I.) Last, we investigate at selected sites the components of temperature changes in the model, integrated over time and averaged over depth:

$$\int_{t=0}^{t=t_{\max}} \overline{T}_t^h dt = \frac{1}{h} \int_{t=0}^{t=t_{\max}} \frac{Q}{\rho c_p} dt + \int_{t=0}^{t=t_{\max}} \left[\overline{(-uT_x - vT_y - wT_z)^h} + \overline{\nabla \cdot (K_h \nabla T)} + \overline{(K_v(z)T_z)^h} \right] dt. \quad (1)$$

(Click the equation graphic to enlarge/reduce size)

The left-hand side in [Eq. \(1\)](#) represents the temperature change from top to depth h due to heat flux Q [surface heat flux minus the (small) solar penetration across depth h], and three-dimensional advection plus horizontal and vertical diffusion. In the advective terms, x , y , and z denote eastward, northward and upward directions; u , \mathbf{u} , and w denote the corresponding velocity components.

In a similar way, we calculated the horizontal momentum budget, integrated over time and averaged over depth h at selected sites:




$$\int_{t=0}^{t=t_{\max}} \overline{\mathbf{u}}_t^h dt = \frac{1}{h} \int_{t=0}^{t=t_{\max}} \frac{\boldsymbol{\tau}}{\rho} dt + \int_{t=0}^{t=t_{\max}} \left[\overline{-\mathbf{u} \cdot \nabla \mathbf{u} - f \mathbf{k} \times \mathbf{u} - \rho_0^{-1} \nabla p^h} + \overline{\nabla \cdot (A_h \nabla \mathbf{u})} + \overline{(A_v(z) \mathbf{u}_z)^h} \right] dt. \quad (2)$$


(Click the equation graphic to enlarge/reduce size)

The vertically averaged time rate of change of velocity is balanced by the surface wind stress $\boldsymbol{\tau}$, advection, Coriolis term (\mathbf{k} is the unit vector in the vertical), horizontal pressure gradient, plus horizontal and vertical friction. Furthermore, to isolate the interannual signal, we removed the mean seasonal cycle from each term in [Eqs. \(1\)](#) and [\(2\)](#), leaving the terms contributing to the temperature anomaly at time t_{\max} , averaged over depth h . When h is the mixed layer depth, the heat balance is directly related to SSTA, though it is sometimes convenient to choose a greater depth (see text for details).

a. Pacific Ocean

1) EQUATORIAL PACIFIC WINDS

Some of the differences between simulated and observed SSTA ([Figs. 5a and 5b](#) ) in the central and eastern Pacific may be due to problems with the winds used. For example, directly measured monthly mean wind stresses along the equator are available for our period of interest at five TAO mooring sites ([Hayes et al. 1991](#)); these are shown in [Fig. 7](#) . We have adjusted TAO wind speeds by a factor of $[\ln(10/z_0)/\ln(4/z_0)]$ because TAO winds are measured at 4 m rather than the standard height of 10 m; the roughness length z_0 of 10^{-7} m is from the [Charnock \(1981\)](#) relation. We have then used the same bulk transfer coefficient of 1.5×10^{-3} that we have used with the FSU pseudostresses. Also shown at each site in [Fig. 7](#)  are wind stresses for the FSU product used in this paper, and for the NCEP reanalysis ([Kalnay et al. 1996](#)).

At each site there are significant differences in mean magnitude between the three products at times when both are available (first three rows, [Table 2](#) ). The (fourth, fifth) rows show the raw rms difference between (FSU, NCEP) and TAO wind stresses at times when all three are available, while the (sixth, seventh) rows show the rms differences between (FSU, NCEP) and TAO when a multiplicative constant is applied to the FSU and NCEP stresses to give them the same mean magnitude as the TAO stresses. Raw FSU winds clearly depart more strongly from TAO than NCEP winds do, especially in the east Pacific. After adjustment to the mean, the discrepancy is reduced.

One notable difference between the products is that FSU winds are substantially larger in magnitude than TAO from June 1989 through January 1990 at 140°W, 125°W, and 110°W, whereas TAO and NCEP winds are closer together at this time. Qualitatively, this difference suggests that when the model is run with the FSU winds we would expect more upwelling in late 1989 in the east Pacific than in a run with NCEP winds; so SST should be colder in a run with the FSU winds. We will return to the question of whether these wind differences are large enough to generate features like the spurious La Niña

2) ANALYSIS OF SURFACE TEMPERATURE IN THE CENTRAL EASTERN PACIFIC

Figure 8a shows the observed (TAO array) and modeled SSTs at (0°, 140°W), and Fig. 8b shows the SSTAs. At this site the model has captured the observed anomalies fairly well: in particular the fall in SSTA at the end of the 1986–87 ENSO event is quite well modeled. However, the rms difference between model and observation is 1.3°C. The tendency for modeled SSTA to have greater magnitude than observed SSTA, independent of sign, probably reflects the problem with the heat flux boundary condition discussed earlier.

Figures 9a,b show modeled and observed temperature anomalies versus depth and time. It is evident from the figures that, both in the model and observation, SSTA is typically of the same sign as the temperature anomaly throughout the top 150 m, while it is typically smaller than anomalies near 100 m, as would be expected from the negative feedback between SSTAs and surface heat fluxes. At this longitude both model and observation SSTA is quite similar to T300A—the average temperature anomaly of the model in the top 300 m (dotted line, Fig. 8b). The T300A anomaly weakly leads SSTA by 0–1 months in the model (Fig. 8c) and the observations (Fig. 8d); correlation coefficients reach 0.9 in the model and 0.77 in the TAO data.

To gain a better insight into the causes of SSTA change, we have examined the point heat budget near 140°W. While this method is harder to check observationally than the volume-average heat budget considered by earlier authors (e.g., Brady and Gent 1994, and references therein; Brady 1994), it gives insights into the processes controlling SST—the quantity that actually affects the atmosphere. We have performed the budget calculation in two ways. In the first, Eq. (1) is taken over the surface mixed layer (defined as the depth at which density exceeds that at 7.5 m by 0.5 kg m⁻³, and marked by the dashed line in Fig. 9a), and second over the top 300 m. Figure 10a shows the progressive time integral of the anomaly of each term in the heat budget Eq. (1), when h is taken as the mixed layer depth [we have not attempted to break the anomalies in the terms of Eq. (1) into individual contributions from anomalies in velocity, temperature gradient, mixed layer depth, etc., since the results then become too complicated to be useful]. The progressive integral of dT/dt is close to the model SSTA, apart from an additive constant, as can be checked by comparison with the full line, Fig. 8b. The surface heat flux term $Q/(h\rho c_p)$ and the diffusive term in Fig. 10a provide small, slowly varying corrections to SSTA, which is mainly controlled (particularly on timescales of a few months or less) by the total advection. Rather surprisingly, vertical and horizontal diffusion are similar in magnitude, and both are small (Fig. 10c). They tend to anti-correlate, presumably because vertical mixing tends to cool the mixed layer while horizontal (i.e., meridional) mixing tends to reduce the equatorial SST minimum. Vertical advection (light blue line, Fig. 10b) is anti-correlated with the net horizontal advection (red line). The difference between them—that is, advection due to the flow component perpendicular to the isotherms—is the only advective component that can actively change SSTA. This type of balance is compatible with the results of Bryden and Brady (1985), who found from analyzing observational data between 150°W and 110°W that, on long-term average, the difference between vertical and horizontal advection is less than half the magnitude of either. The biggest change in SSTA—a cooling in mid-1988, Fig. 10a—occurs when the anticorrelation of vertical and horizontal advection breaks down. The heat budget for the top 300 m (not shown) is simpler, but the basic conclusion is still valid: namely, that the largest changes in SSTA occur when the near-balance of vertical and horizontal advection breaks down seriously and cross-isopycnal flow develops.

Ideally, one would like to explore this further, to find an empirical rule relating the occurrence of cross-isopycnal flow to details of the wind forcing. Unfortunately, this seems to be difficult: for example, Fig. 11 shows the zonal velocity anomaly at (0°, 140°W), from the model and from current meter observations (TOGA/TAO). In both model and observations, there is a strong tendency for anomalies in u to have the same sign at all depths, suggesting that these anomalies are mainly a lowest baroclinic mode phenomenon. However, comparison of Fig. 9 with Fig. 11 suggests that at 140°W, the model does not reproduce the observed time dependence of u as well as it does of T .

Figure 12a shows the zonal momentum balance for the mixed layer. The velocity anomaly in the mixed layer (red line) is the sum of four terms, three of which are typically larger in magnitude than their sum, and there is little clear correlation between them. No single pair of terms can be identified as the primary balance for the whole period of record, even to crude approximation. Three of the terms in Fig. 12a are, in turn, fairly complex sums: advection term (Fig. 12b), diffusion term, and total zonal pressure gradient term (not shown). This may explain the model's relative lack of success in simulating the observed anomalies of zonal velocity at 140°W (Fig. 11). Such results do not encourage the idea that there is a simple rule relating

$$u \, dT/dx + v \, dT/dy + w \, dT/dz,$$

the prime contributor to SST change on the timescale of a few months, to the applied forcing. Similar conclusions are reached by averaging the zonal momentum budget over the top 300 m.

3) ANALYSIS OF SURFACE TEMPERATURE IN THE FAR EASTERN PACIFIC

Figures 13–17 are the equivalents of Figs. 8–12, but at 110°W. Modeled SST and SSTA (Figs. 13a,b) now show fluctuations with timescales of a few months, which are much larger than observed; there is little correlation between observed and modeled temperatures. Note the different vertical scales from Fig. 8. T300A (dotted line, Fig. 13b) is intermediate in properties between observed and modeled SSTA; its maximum correlation with each (Figs. 13c,d) is only slightly less than in Figs. 8c,d, but it stays at high levels for shorter periods. Comparison of Figs. 14a,b shows that

(as at 140°W) the model captures the vertical structure of temperature changes quite well. As expected from Figs. 5 and 13, the anomaly timescales are too short in the model, and large departures from observation are seen in late 1985 and late 1989 at all depths.

The mixed-layer heat budget at 110°W (Fig. 15) shows some major differences from 140°W. In the former, no term was much larger than the time-integrated rate of change of temperature. In the latter, the rate of change term is a small residual from a primary balance in which total advection balances net surface heat flux/mixed layer depth. Note that the mixed layer depth is typically 20 m deep at 110°W, and more like 60 m deep at 140°W (dashed lines, Figs. 9a and 14a), which accounts for the large magnitude of the “source” term in Fig. 15. As at 140°W, the major changes in SSTA on timescales of a few months (red line, Fig. 15a) are mainly set by changes in the total advection. Also as at 140°W, the net horizontal advection (red line, Fig. 15b) anti-correlates with vertical advection (light blue line); however, because each of these is so large, only small relative differences between these two terms result in significant changes in SST in Fig. 15a.

The momentum balance (Fig. 16) shows that, to an even greater extent than at 140°W, the zonal velocity within the mixed layer is the small residual of a number of large terms. Once again, it is the small mixed layer depth that is responsible for the large magnitude of the “ τ_x ” term (actually τ_x /mixed layer depth) at 110°W. It is therefore not surprising that the model is again not very successful in simulating anomalies of zonal velocity (Fig. 17). However, as in Fig. 12 the model reproduces the vertical structure of anomalies fairly well.

4) POSSIBLE CAUSES OF SST DISCREPANCIES IN THE EQUATORIAL PACIFIC

To summarize the above results, our budget at 140°W shows that the strongest single event in the SSTA time series—a rapid cooling in mid-1988—is almost purely advective in origin and can be traced (in the model) to a burst of upwelling that coincided with strong easterlies at all longitudes west of 140°W (Fig. 7), especially in the FSU winds we used. We have not been able to trace the source of this cooling back to local wind stresses (τ_x term in Fig. 12a); it appears remotely driven by wind stresses in the western Pacific.

Such an identification is even more difficult at 110°W. The results of the last two sections suggest that prediction of SST may become more sensitive to errors in forcing functions with distance east because, as the mixed layer decreases, surface temperature and velocity are determined by a progressively finer balance of terms.

Kessler and McPhaden (1995, hereafter KMCP) studied the SST dynamics extensively at 140°W, using TAO data, and found a relation between low-pass filtered values of observed zonal wind stress τ_x , depth z_{23} of the 23°C isotherm, and SST, at 140°W:

$$\text{SST} = A \frac{\tau_x}{\rho z_{23}} + T_0. \quad (3)$$

All quantities are low-pass filtered with a half-power point of about 5 months before insertion in Eq. (3). The relationship (3) is empirical, but it expresses the idea that the depression of SST below the value T_0 (which it would have if local wind stresses, τ_x were absent) is proportional to the strength of wind-driven upwelling (i.e., to τ_x) and to the temperature of upwelled water, which is assumed to be governed by the depth of an isotherm just below the mixed layer. KMCP found that the estimate (3) correlated at 0.9 with observed SST over 1985–93; A was $4.6 \times 10^6 \text{ }^\circ\text{C m}^{-1} \text{ s}^{-2}$; and T_0 was 29.3°C. We tested it over 1985–90, and found that in model data, the singularity in (3) as z_{23} approaches zero leads to strongly nonlinear behavior in our estimate, even though the model and observed z_{23} are not grossly different from one another.

Nevertheless, Eq. (3) can be used to estimate the likely effect of errors in zonal wind stresses of a given magnitude. Figure 7 shows that different wind products can differ by up to 0.04 N m⁻² for several months (e.g., at 140°W in late 1989). Insertion of a wind “error” of this magnitude in (3) with a typical value for z_{23} of 50 m yields an SST “error” of about 4°C. If (as seems reasonable) the TAO directly measured winds were given more weight than the FSU winds, one would conclude that use of the FSU winds would lead to errors of this magnitude at 140°W. We obtained SST errors of about this magnitude in late 1989—but not at 140°W (Fig. 8); they become strong about 500–1000 km farther east (Fig. 5). This suggests that the use of a strictly local wind stress in (3) may not be appropriate.




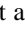

As noted earlier, similar to our results Davey et al. (1994) and Brady (1994) also obtained incorrect SSTAs in 1989–90. Brady’s SSTAs were not as far from observation during the spurious cold event of late 1989 as those of Davey et al. or ours. This may be because the mixed layer in her model was 50 m deep, while ours narrowed to only 25 m in late 1989 (dashed line, Fig. 14a). We showed in section 3a(c) that the (realistic) thinning of the mixed layer in the east Pacific causes SST to become more sensitive, in the sense that SST change is a small residue of large, compensating terms. A reasonable interpretation of these results is (i) that the FSU winds may indeed have substantial errors in much of the eastern equatorial Pacific in the second half of 1989, as suggested by Fig. 7 and the consistency of three model’s SSTA results, and (ii) the use of realistic mixed layer depths may enhance the sensitivity of modeled SSTAs in the east Pacific to small wind errors, resulting in the large errors in SSTA seen in Figs. 5 and 13. However, uncertainties in model physics are

such that other interpretations are still possible.

To validate our claim that the FSU winds have errors in late 1989, we performed a sensitivity experiment where we reduced the wind stress vectors in the eastern Pacific in late 1989 by a factor of 0.75. This caused much smaller SSTAs in late 1989 and SSTAs were generally much closer to observations (Y.-L. Zhang 1998, personal communication).

5) A TEST OF DELAYED-OSCILLATOR PHYSICS IN THE MODEL




[Picaut et al. \(1996\)](#) used averaged currents between 4°N and 4°S in the equatorial Pacific over 1982–94 to plot positions of “hypothetical drifters” advected by these currents. They used observations from current meters, surface drifters, and satellite altimetry and compared them to three different models. The trajectories can be interpreted as zonal displacements of water masses along the equatorial band, which results from the integration in space and time of the surface currents within 4°N to 4°S. For each current, drifters converge on a front, which moves quite accurately back and forth with the SOI.

We repeated Picaut et al.’s drifter calculation with our model’s surface current ([Fig. 18](#) ); our “drifters” were released between 140°E and 140°W with an interval of 20°. We find that our trajectory fits on Picaut et al.’s observed data (their [Fig. 2](#) ). It is obvious from [Fig. 18](#)  that after about one year these drifters converge to a single line, which represents the eastern edge of the warm pool. Furthermore, the converged tracks very much resemble the signal of the SOI (thick line in [Fig. 18](#) ). Based on their results, Picaut et al. conclude that zonal advection of temperature is the dominant mechanism that determines the zonal migration of the eastern edge of the warm pool over the entire period 1986–94. However, as is the case with their results, we too find that there is an exception to this conclusion during the 1988–89 La Niña when strong westward currents yielded trajectories that were too far westward (probably because processes other than zonal advection effect SST). The general agreement with Picaut et al.’s work confirms our previous finding that, despite that at 140°W our model does not reproduce observed zonal velocity anomalies ([Fig. 11](#) ) as well as it does temperature anomalies, the basic current structure is in close agreement with observations.


By calculating hypothetical drifters for the depth-averaged velocities from top to 350 m we tried to investigate if the convergence of the trajectories is restricted to the surface or if it applies to the thermocline as well. The model does not reproduce the nice convergence feature; the most likely explanation is the Equatorial Undercurrent, which does not show a convergence like the surface currents. However, a simple time integral of the depth-averaged current at 140°E near the western boundary depicts a clear correlation with the zonal movements of the convergence zone, lagged by about 6 months (not shown). This is qualitatively as expected from “delayed oscillator” theory [see [Neelin et al. \(1998\)](#) for a review of this theory]. Results from a slightly different, 16-yr run of our model confirms the robustness of this result. The details of this phenomenon, including nonlinear effects not usually treated in delayed oscillator theory, will be explored in another paper, in preparation.

b. Indonesian Throughflow

1) ANALYSIS OF SURFACE TEMPERATURE ALONG THE THROUGHFLOW

This site is distinct from the previously investigated sites in two respects. First, it is within the Indonesian archipelago along the axis of the main throughflow. Second, it is close to the center of the simulated tidal mixing in our model (see paper I). The model has a distinct semiannual signal in the top 100 m, whereas the observations show it down to 450 m (not shown). The amplitude of the interannual signal in the ITF is much smaller than in the two sites previously investigated in the Pacific. [Figures 19a,b](#)  show that sometimes the sign of SSTA is anti-correlated with subsurface temperature anomalies in both the model and observations. In the model, this is caused by local heat flux variations of seasonal timescale felt by SSTA but not by subsurface temperature anomalies. The depth versus time plots of potential temperature anomalies reveal an ENSO-related interannual signal with a weak negative anomaly centered at a depth of about 150 m in 1986/87 (El Niño) and a positive anomaly centered at the same depth for 1988/89 (La Niña). The XBT data show a less clear signal, but the anomalies below 150 m reveal the same sequence of positive and negative variability (no observations before August 1986 were available, which may cause a bias when comparing the anomalies). Obviously, the semiannual monsoonal impact on SST is much stronger than the interannual variability, confined to depths well below the mixed layer. This result is supported by [Figs. 3a](#)  and [4](#) : the first EOF of SSTA in this area hardly depicts any ENSO-related signal, but a strong first EOF signal in upper-ocean heat content (450 m) indicates a strong response to ENSO.

The cumulative anomalies of temperature at (8°S, 124°E) integrated over the mixed layer depth (not shown) reveal large contributions from surface-flux anomalies. However, advection and diffusion show similar amplitudes, and all of those terms are larger than the temperature anomaly itself. Therefore, one can expect that there will be many terms contributing to local heat anomalies and hence the complicated patterns we find there. This result confirms the special character of this region as a western boundary current regime (the ITF).

The enhanced vertical diffusion caused by the simulated tidal mixing near this particular site transforms to a mean vertical temperature decrease of 0.8°C. This implies a mean heat loss of about 50 W m⁻² through the base of the mixed layer (mean depth 45 m, [Fig. 19a](#) ) in close agreement with observation-based estimates ([Field and Gordon 1996](#)). Although there is an interannual signal in the tidally induced vertical mixing, other terms in the heat balance are of similar magnitude. Thus no simple relationship between tidally induced mixing and SSTA can be deduced.

2) ANALYSIS OF SURFACE TEMPERATURE NORTHWEST OF AUSTRALIA

We compared observations from the XBT line Fremantle (Australia)–Sunda Strait (Java) in the eastern Indian Ocean (Meyers 1996) with our model results. Figure 20 shows Hovmoeller diagrams for the deviations from the mean of the depth of the 20° isotherm D_{20} (Figs. 20a,b), the anomalies of D_{20} (Figs. 20c,d), and the anomalies of SST (Figs. 20e,f). Figures 20a,b contain all the variability including annual and semiannual signals (the mean was subtracted), whereas the anomalies displayed in Figs. 20c–f were calculated by subtracting the mean seasonal cycle from both datasets. The interannual signal in the observations (D_{20} and SST) is strongest toward the southern end of the section.

Likewise, the model simulation shows strong interannual signals there. Observations and model both reveal an anomalously shallow thermocline during 1986–87 developing with negative SSTAs, which indicates El Niño conditions. An anomalously deep thermocline developed during 1988–89 associated with positive SSTAs (La Niña condition) (Meyers 1996). In contrast to the observations, the model shows a much stronger semiannual component along the coast of Java in all three figures. This signal is caused by the South Java Current as an extension to the semiannual equatorial Wyrтки jet. The northernmost bin for the XBT data (6.5°S to 8°S) is too coarse to capture this signal. On the other hand, the model lacks sufficient horizontal resolution toward the southern end of the IX1 line (resolution about 2° × 3°) to capture signals that are smaller than the model's grid size but are apparent in the observations. The section-averaged correlations between model and data reveal moderate correlations of about 0.5 for D_{20} arrays and a correlation of 0.6 for SSTAs.

Using data from the Semtner and Chervin (1992) model, Qu et al. (1994) investigated the seasonal heat budget in the upper 50 m along the IX1 XBT line. They found strong annual mean upwelling in the northern part and weak annual mean downwelling in the southern part. In both regions, annual variations are driven by local wind stresses. In the northern part remotely forced semiannual variations also contribute to vertical motions of the thermocline; the annual-mean surface heat flux and advection are an order of magnitude smaller than those in the seasonal budget (however, tidal mixing was not included in their model). Cold upwelling is largely canceled by warm advection from the ITF. In the southern region the primary control on the seasonal variation on SST is the surface heat balanced by advection from the ITF.

Our interannual results complement Qu et al.'s (1994) seasonal analysis. In the northern part of the line neither the model results nor the observations show ENSO-related variability; it is therefore not investigated here. For the southern region we chose a site along the Fremantle–Sunda Straits XBT line at 23°S, 112°E, that is, in the southern part of the line. Figure 21a reveals that modeled and observed SSTs are controlled by the annual cycle. However, a weak interannual signal associated with ENSO is apparent in all SSTAs (Fig. 21b). Model and observations differ, on average, by less than 0.5° C, but the differences among the three datasets are of the same size as their anomalies. Note that typical differences between the two observed SST datasets—the XBTs and Reynolds data—are often comparable to the difference between the model SST and either observed product.

As with SST, the upper 100 m of the water column and the associated mixed layer depth (annual mean depth: 70 m) have an annual cycle with homogenous mixing near the surface in austral winter (September) and high SSTs/low mixed layer depths in austral summer (February–March). A similar picture for temperature evolves from the observations (not shown). The vertical and temporal extension of the anomalies in Figs. 22a,b depict similarities to the same quantities in the Indonesian archipelago (Figs. 19a,b). But now in both model and observations the (smaller) anomalies extend almost always to the surface, in contrast to the previous site. As with sites in the Pacific, the deep temperature anomalies in both model and observations are a good guide to SSTAs. In the model, deep temperature anomalies are weakly leading SSTA by one month, whereas the reverse happens in the observations (Figs. 21c,d).

The time rate of change of accumulated temperature anomalies in the mixed layer (not shown) is clearly dominated by anomalous cold vertical advection from late 1986 through to early 1988, with the reverse happening from late 1988 to early 1990. Both signals indicate the arrival of the ENSO signal along the northwest Australian coast with a reduced (increased) thermocline thickness during the El Niño (La Niña). The source of this anomalous upwelling is likely to be associated with Kelvin waves that emanate from the tip of Irian-Jaya and then propagate along Australia's northwest coast (Clarke and Liu 1994). We would like to point out that SSTA at 23°S, 112°E in the model is determined by a balance between anomalous vertical advection and slowly varying total diffusion. The only exception is in 1988 when positive heat flux anomalies get as large as the other terms in the heat budget and accelerate the transitions from cold to warm anomalies. These results are in contrast to the seasonal signal (Qu et al. 1994) where local Ekman transport balances the net heat fluxes. Although the ENSO events appear in both model and observations, we are probably missing some local dynamics, which comes through in the not very impressive agreement in SSTAs (Fig. 21b).

3) INDIAN OCEAN: ANALYSIS OF SURFACE TEMPERATURE IN THE CENTRAL EQUATORIAL INDIAN OCEAN

The site in the equatorial Indian Ocean contains a small interannual signal superimposed on the semiannual cycle of the surface fields. The mixed layer depth (annual mean depth at about 48 m) is predominantly determined by monsoonal frequencies (not shown). Variability is mainly restricted to the upper 200 m of the water column in both model and observations (Figs. 23a,b). In the model, temperature anomalies are largest at about 70 m and show strong variability at frequencies of about twice a year, probably associated with interannual variability of the Wyrтки jet. Qualitatively similar behavior is seen in the observations (Fig. 23b). In both model and observations, SSTAs are positively correlated with those over the top 70 m (model: 0.63, observations: 0.60). At this site in the Indian Ocean no ENSO-related signal could be found in the model.

The impact of interannual shortwave radiation on SST anomalies in the Indian Ocean was investigated by performing an additional model run with mean seasonal shortwave radiation but interannual wind stress forcing. In the equatorial and northern Indian Ocean the major effect of interannually net solar shortwave radiation (maximum variability $\pm 40 \text{ W m}^{-2}$) is

an increase in the amplitude of SST variability of up to 1°C. During the 1986–87 El Niño (1988–89 La Niña) SSTAs with interannual solar shortwave radiation are higher (lower) than with seasonal solar shortwave radiation. South of the equator this effect is modulated by the ITF signal and the impact of solar shortwave radiation becomes less apparent. The associated variability in total heat flux can almost completely be ascribed to the solar shortwave radiation. The changes in latent/sensible heat flux and longwave radiation due to enhanced variability in SSTA are less than 10 W m^{-2} in total. However, the small magnitude of SSTAs caused by interannual shortwave radiation is similar in magnitude to the wind-driven variability and thus represents an important contribution to SSTA in the equatorial Indian Ocean, the Bay of Bengal, and the Arabian Sea ([Murtugudde and Busalacchi 1999](#)). However, a quantitative assessment of the impact of interannual solar shortwave radiation on SSTA is rather difficult because it depends on three error-prone components: the solar shortwave radiation itself, the heat flux parameterization, and the small amplitude of (observed) interannual SST variability in the Indian Ocean.


4. Summary and discussion

A global ocean circulation model driven by interannually variable fluxes of wind stress and solar shortwave radiation was used to study SST and upper-ocean variability between 1985 and 1990. Because SST and its anomalies are determined by temporal variations in ocean–atmosphere fluxes, advection, and diffusion, we investigated the heat budget in the upper ocean as a function of time. We find that our model does a reasonable job in simulating observed temperature variabilities in the upper oceans. Over much of the tropical Pacific and Indian Oceans, modeled and observed ([Reynolds and Smith 1994](#)) SSTAs are positively correlated; in a large area in the Pacific they exceed 0.6. However, the model overestimates the meridional extent of SST variability in the equatorial Pacific and the corresponding amplitude in parts of the Pacific and Indian Oceans. EOF analyses for SSTA and upper-ocean heat content revealed the dominating influence of ENSO, which extends via the ITF and by atmospheric circulation into the Indian Ocean.

Comparison of observed and simulated phases of interannual temperature variability in the upper 450 m confirmed that the model's simulation is reasonable. However, almost all of the sites investigated indicate that our upper thermocline is too warm. This suggests that horizontal and vertical diffusion should be improved in future versions of the model, but it did not seriously affect the anomalies. On the other hand, SSTAs were affected by our choice of heat flux boundary condition, with the ratio of air humidity to saturated humidity over freshwater at SST in the latent heat flux term being independent of the spatial scale of the SSTA pattern. This implied a weaker negative feedback on SST change and thus larger than observed SSTAs.

In the central Pacific at (0° , 140°W), budgets of temperature anomalies over the surface mixed layer and over the top 300 m both show the primary causes of temperature change to be zonal and vertical advection, with their sum generally less than half of either term individually. Our model, in common with other ocean models, fails to simulate SST variability in the eastern Pacific. At (0° , 110°W), the mixed layer is much thinner (minimum depth at about 25 m) so that the temperature changes are a small disturbance to a basic balance between the vertical convergence of heat flux and vertical and zonal advection. At both sites the zonal flow (and hence the zonal heat advection) is in turn determined by a sum of several terms, none of which are small. It is therefore difficult to find a clear physical basis in our model for the [Kessler and McPhaden \(1995\)](#) empirical rule for SSTAs, which correlates strongly with observed SSTAs. However, this rule suggests that differences between wind stress products that exceed 0.04 N m^{-2} over several months (as occurs at 0° , 140°W in 1989) could lead to differences in SSTAs of up to 4°C . This may help explain why a short but intense La Niña episode occurred in our model, but not in the observed SST. Comparison with other model results ([Brady 1994](#); [Davey et al. 1994](#)) and a sensitivity experiment with reduced wind stresses tend to confirm that the FSU winds were in error in the east Pacific in late 1989, and suggests that the use of a realistic (thin) surface mixed layer exacerbates the problem by strengthening the sensitivity of SSTAs to wind errors. A similar conclusion about the feedback between realistic mixed layer depths and surface heat fluxes in equatorial upwelling regions was drawn by [Murtugudde et al. \(1996\)](#). They achieved increased realism in modeling the ocean mixed layer by using an advective–diffusive atmospheric boundary layer model.

Enhanced vertical diffusion due to simulated tidal mixing in the Indonesian archipelago causes a mean heat loss of 0.8°C (about 50 W m^{-2}) through the base of the mixed layer; this agrees closely with observationally based estimates. The interannual signal in the tidally induced mixing is of similar magnitude to other terms and hence does not dominate the anomalous heat balance. Variability in the top 100 m of the water column in the Indonesian region (8°N , 124°E) has a predominantly semiannual character; interannual variability is mainly confined to depths below the mixed layer. ENSO-related interannual signals with a weak negative anomaly centered at a depth of about 150 m in 1986–87 (El Niño) and a positive anomaly centered at the same depth for 1988–89 (La Niña) are very similar to the observed (XBT) data.

Both model and XBT observations along the IX1 section show strong similarities in the depth of the 20°C isotherm and SSTA during 1985–90. Section-averaged correlations are 0.5 and 0.6 for D_{20} anomalies and SSTAs, respectively. Larger discrepancies are caused by opposite model grid resolution and data sampling density at both boundaries. SST close to the southern end of this section at 23°S , 112°E is dominated by the annual signal with a superimposed weak interannual signal. The vertical and temporal extension of the temperature anomalies in the top 450 m depict similarities to the Indonesian archipelago (as could be expected from the EOF of heat content, [Fig. 4a](#) ). In both model and observations the smaller anomalies at 23°S , 112°E extend almost always to the surface, in contrast to the Indonesian site. The time rate of change of accumulated temperature anomalies in the top 450 m is dominated by anomalous cold vertical advection from late 1986 through to early 1988, with the opposite happening from late 1988 through to early 1990. Both signals indicate the arrival of the ENSO signal along the northwest Australian coast with a reduced (increased) thermocline thickness during the El Niño (La Niña) event. SSTA at 23°S , 112°E in the model is determined by a balance between anomalous vertical advection and slowly varying total diffusion, with the exception of 1988 when positive heat flux anomalies accelerate the transition from

negative SSTA (El Niño condition) to positive SSTA (La Niña condition).

SSTAs in the central Indian Ocean (0°, 66°E) are typically of the order of 0.5°C. However, subsurface anomalies can be larger than 2°C. Variability is mainly restricted to the upper 200 m of the water column in both model and observations. In the model, temperature anomalies are largest at about 70 m and show strong variability at frequencies of about twice per year, probably associated with interannual variability of the Wyrki jet. Another possible mechanism is that Ekman pumping associated with the local wind forcing drives the thermocline movement (Murtugudde et al. 1998). A sensitivity experiment with interannually instead of seasonally variable solar shortwave radiation over the Indian Ocean increased the amplitude of SST anomalies up to 1°C in the tropical and northern Indian Ocean.

From examining the heat budget of the surface mixed layer at all the locations shown in Fig. 6, we concluded:

- In all locations, the model reproduces the observed vertical structure of temperature anomalies fairly well, even when it does not reproduce the observed SSTA time series well. In locations where temperature anomalies are usually of one sign over the top few hundred meters, heat budgets that extend well below the mixed layer may be more informative of the process governing SSTAs than mixed-layer heat budgets.
- In all locations examined except one (0°, 110°E, where there is a model physics problem), the surface heat flux term is not the *dominant* term in the anomaly heat budget for the surface mixed layer (though it is not negligible anywhere). Advection is usually the largest term. This result is rather surprising away from regions with strong currents; it suggests that the inadequacies of present interannually varying heat flux products may not be as serious a limitation to modeling SSTAs as previously thought. On the other hand, it places greater emphasis on the need for accurate wind stress products.

There are some caveats with our findings: First, we investigated a relatively short period of just six years (mainly because of the lack of reliable solar shortwave radiation data—see paper I). The anomalies may be biased by other ocean–atmosphere phenomena such as the quasi-biennial oscillation (e.g., Meehl 1993). One of the referees suggested that the likely error in the FSU winds makes it very difficult to simulate the “decadal” shift that is supposed to have occurred during this period (e.g., Gu and Philander 1997).

Although two major ENSO events are captured by our simulation period, we must be cautious about suggesting that the discussed term balance anomalies are representative for all ENSO periods. Furthermore, our model is forced by observations derived from different sources and different data processing procedures have been applied to those fields. This might hamper the spreading and detection of teleconnections between, for example, the Pacific and Indian Oceans in contrast to a full ocean–atmosphere coupled model.

We concentrated on temperature as the dominant thermodynamical signal in the tropical regions of the oceans. However, recent research has demonstrated the importance of salinity perturbations in tropical ocean dynamics and thermodynamics (Vialard and Delecluse 1998a,b). Murtugudde and Busalacchi (1998) showed that salinity changes the area of the warm pool and affects the cold tongue in the Pacific; that is, the zonal SST gradient is smaller when salinity and observed freshwater fluxes are included.

Future versions of the model will focus on better representation of surface forcing fields by using daily rather than monthly mean winds with an atmospheric boundary layer model, an improved freshwater flux formulation, a finer grid resolution, and a larger flux dataset.

Acknowledgments

Susan Wijffels and two anonymous reviewers made numerous helpful suggestions to improve the manuscript. The data from the TOGA buoys were made available to us by Nancy Soreide, Dai McClurg, and Linda Mangum from PMEL. Jim Mansbridge installed these data on our local computer network. The processed XBT data for the Indian Ocean and Indonesian Throughflow were provided by Lidia Pigot. Most of the figures were prepared with the public domain software package FERRET from PMEL. The project is largely supported by funding from the CSIRO Division of Marine Research and the Land & Water Resources Research and Development Corporation, Australia.

REFERENCES

Brady, E. C., 1994: Interannual variability of meridional heat transport in a numerical model of the upper equatorial Pacific Ocean. *J. Phys. Oceanogr.*, **24**, 2675–2694. [Find this article online](#)

— and P. R. Gent, 1994: The seasonal cycle of meridional heat transport in a numerical model of the Pacific equatorial upwelling zone. *J. Phys. Oceanogr.*, **24**, 2658–2673. [Find this article online](#)

Bryden, H. L., and E. C. Brady, 1985: Diagnostic model of the three-dimensional circulation in the upper equatorial Pacific Ocean. *J. Phys. Oceanogr.*, **15**, 1255–1273. [Find this article online](#)

Charnock, H., 1981: Air–sea interaction. *Evolution of Physical Oceanography*, B. A. Warren and C. Wunsch, Eds., The MIT Press, 482–

Chen, D., A. J. Busalacchi, and L. M. Rothstein, 1994a: The roles of vertical mixing, solar radiation, and wind stress in a model simulation of the sea surface temperature seasonal cycle in the tropical Pacific Ocean. *J. Geophys. Res.*, **99**, 20 345–20 359..

— —L. M. Rothstein, and A. J. Busalacchi, 1994b: A hybrid vertical mixing scheme and its application to tropical ocean models. *J. Phys. Oceanogr.*, **24**, 2156–2179.. [Find this article online](#)

Clarke, A. J., and X. Liu, 1994: Interannual sea level in the northern and eastern Indian Ocean. *J. Phys. Oceanogr.*, **24**, 1224–1235.. [Find this article online](#)

Davey, M. K., S. Ineson, and M. A. Balmaseda, 1994: Simulation of hindcasts of tropical Pacific Ocean interannual variability. *Tellus*, **46A**, 433–447..

Drosowsky, W., 1993: An analysis of Australian seasonal rainfall anomalies: 1950–1987. Part I: Spatial patterns. *Int. J. Climatol.*, **13**, 1–30..

Ffield, A., and A. L. Gordon, 1996: Tidal mixing signatures in the Indonesian Seas. *J. Phys. Oceanogr.*, **26**, 1924–1937.. [Find this article online](#)

Gent, P. R., and M. A. Cane, 1989: A reduced gravity, primitive equation model for the upper equatorial ocean. *J. Comput. Phys.*, **81**, 444–480..

Godfrey, J. S., 1996: The effect of the Indonesian Throughflow on ocean circulation and heat exchange with the atmosphere: A review. *J. Geophys. Res.*, **101**, 12 217–12 237..

Gu, D., and S. G. Philander, 1997: Interdecadal climate fluctuations that depend on exchanges between the Tropics and extratropics. *Science*, **275**, 805–807..

Hayes, S., L. Mangum, J. Picaut, A. Sumi, and K. Takeuchi, 1991: TOGA–TAO: A moored array for real-time measurements in the tropical Pacific Ocean. *Bull. Amer. Meteor. Soc.*, **72**, 339–347.. [Find this article online](#)

Hellerman, S., and M. Rosenstein, 1983: Normal monthly wind stress over the world ocean with error estimates. *J. Phys. Oceanogr.*, **13**, 1093–1104.. [Find this article online](#)

Hirst, A. C., and J. S. Godfrey, 1994: The response to a sudden change in Indonesian Throughflow in a global ocean GCM. *J. Phys. Oceanogr.*, **24**, 1895–1910.. [Find this article online](#)

Kalnay, E., and 21 Co-authors, 1996: The NCEP/NCAR 40-Year Reanalysis Project. *Bull. Amer. Meteor. Soc.*, **77**, 437–471.. [Find this article online](#)

Kessler, W. S., and M. J. McPhaden, 1995: The 1991–1993 El Niño in the central Pacific. *Deep-Sea Res.*, **42**, 295–333..

Kleeman, R., and S. B. Power, 1995: A simple atmospheric model of surface heat flux for use in ocean modeling studies. *J. Phys. Oceanogr.*, **25**, 92–105.. [Find this article online](#)

Legler, D. M., I. M. Navon, and J. J. O'Brien, 1989: Objective analysis of pseudostress over the Indian Ocean using a direct-minimization approach. *Mon. Wea. Rev.*, **117**, 709–720.. [Find this article online](#)

Levitus, S., R. Burgett, and T. Boyer, 1994: *World Ocean Atlas 1994*. Vol. 3: *Salinity*, NOAA Atlas NESDIS 3, U.S. Department of Commerce, National Oceanic and Atmospheric Administration, p. 99..

Li, Z., 1995: Intercomparison between two satellite-based products of net surface shortwave radiation, *J. Geophys. Res.*, **100**, 3221–3232..

Meehl, G. A., 1993: A coupled air–sea biennial mechanism in the tropical Indian and Pacific regions: Role of the ocean. *J. Climate*, **6**, 31–41.. [Find this article online](#)

Meyers, G., 1996: Variation of Indonesian Throughflow and the El Niño–Southern Oscillation. *J. Geophys. Res.*, **101**, 12 255–12 263..

Molcard, R., M. Fioux, and A. G. Ilahude, 1996: The Indo–Pacific throughflow in the Timor Passage. *J. Geophys. Res.*, **101**, 12 411–12 420..

Murtugudde, R., and A. J. Busalacchi, 1998: Salinity effects in a tropical ocean model. *J. Geophys. Res.*, **103**, 3283–3300..

— —and — —1999: Interannual variability of the dynamics and thermodynamics of the tropical Indian Ocean. *J. Climate*, **12**, 2300–2326.. [Find this article online](#)

— —R. Seager, and A. J. Busalacchi, 1996: Simulation of the tropical oceans with an ocean GCM coupled to an atmospheric mixed layer model. *J. Climate*, **9**, 1795–1815.. [Find this article online](#)

— —A. J. Busalacchi, and J. Beauchamp, 1998: Seasonal-to-interannual effects of the Indonesian throughflow on the tropical Indo-Pacific Basin. *J. Geophys. Res.*, **103**, 21 245–21 441..

Neelin, N. D., D. S. Battisti, A. C. Hirst, F.-F. Jin, Y. Wakata, T. Yamagata, and S. E. Zebiak, 1998: ENSO theory. *J. Geophys. Res.*, **103**, 14 261–14 290..

Nicholls, N., 1989: Sea surface temperatures and Australian winter rainfall. *J. Climate*, **2**, 965–973.. [Find this article online](#)

—, 1996: Modelling climatic variability. *Climate Change: Developing Southern Hemisphere Perspectives*, T. Giambelluca and A. Henderson-Sellers, Eds., Wiley and Sons, 131–143..

Picaut, J., M. Ioualalen, C. Menkes, T. Delcroix, and M. J. McPhaden, 1996: Mechanism of the zonal displacements of the Pacific warm pool: Implications for ENSO. *Science*, **274**, 1486–1489..

Power, S. B., R. Kleeman, R. A. Colman, and B. J. McAvaney, 1995: Modeling the surface heat flux response to long-lived SST anomalies in the North Atlantic. *J. Climate*, **8**, 2161–2180.. [Find this article online](#)

Qu, T., G. Meyers, J. S. Godfrey, and D. Hu, 1994: Ocean dynamics in the region between Australia and Indonesia and its influence on the variation of sea surface temperature in a global general circulation model. *J. Geophys. Res.*, **99**, 18 433–18 445..

Reynolds, R. W., 1988: A real-time global sea surface temperature analysis. *J. Climate*, **1**, 75–86.. [Find this article online](#)

—, and T. M. Smith, 1994: Improved global sea surface temperature analyses using optimum interpolation. *J. Climate*, **7**, 929–948.. [Find this article online](#)

Schiller, A., J. S. Godfrey, P. C. McIntosh, G. Meyers, and S. E. Wijffels, 1998: Seasonal near-surface dynamics and thermodynamics of the Indian Ocean and Indonesian Throughflow, in a global ocean general circulation model. *J. Phys. Oceanogr.*, **28**, 2288–2312.. [Find this article online](#)

Seager, R., S. E. Zebiak, and M. A. Cane, 1988: A model of the tropical Pacific sea surface temperature climatology. *J. Geophys. Res.*, **93**, 1265–1280..

—, M. B. Blumenthal, and Y. Kushnir, 1995: An advective atmospheric mixed layer model for ocean modeling purposes: Global simulation of surface heat fluxes. *J. Climate*, **8**, 1951–1964.. [Find this article online](#)

Semtner, A. J., and R. M. Chervin, 1992: Ocean general circulation from a global eddy resolving model. *J. Geophys. Res.*, **97**, 5493–5550..

Stockdale, T., D. Anderson, M. Davey, P. Delecluse, A. Kattenberg, Y. Kitamura, M. Latif, and T. Yamagata, 1993: TOGA Numerical Experimentation Group. Intercomparison of tropical ocean GCMs. World Climate Research Programme, Tech. Doc. WCRP-79 - WMO/TD 545, 88 pp..

Stricherz, J., J. O'Brien, and D. Legler, 1992: *Atlas of Florida State University Tropical Pacific Winds for TOGA 1966–1985*, The Florida State University, p. 256..

Trenberth, K. E., 1996: El Niño–Southern Oscillation. *Climate Change: Developing Southern Hemisphere Perspectives*, T. Giambelluca and A. Henderson-Sellers, Eds., Wiley and Sons, 145–173..

Vialard, J., and P. Delecluse, 1998a: An OGCM study for the TOGA decade. Part I: Role of salinity in the physics of the western Pacific fresh pool. *J. Phys. Oceanogr.*, **28**, 1071–1188.. [Find this article online](#)

—, and —, 1998b: An OGCM study for the TOGA decade. Part II: Barrier-layer formation and variability. *J. Phys. Oceanogr.*, **28**, 1089–1106.. [Find this article online](#)

WMO, 1995a: *Proceedings of the International Scientific Conference on the Tropical Ocean Global Atmosphere (TOGA) Programme*. Vols. I and II, WCRP-91-WMO/TD No. 717, 911 pp..

—, 1995b: The global climate system review. Climate system monitoring. June 1991–November 1993. WMO No. 819, 150 pp..

—, 1996: WCRP workshop on air–sea flux fields for forcing ocean models and validating GCMs. WCRP-95-WMO/TD No. 762, 184 pp..

Tables

Table 1. Model resolution, surface boundary conditions, and experiment.

--

Freshwater flux:	Newtonian restoring to Levitus et al. (1994) data
Special features:	Hybrid mixed layer model (Chen et al. 1994b; Power et al. 1995); increased vertical diffusion and viscosity in Indonesian archipelago to simulate tidal mixing
Integration period:	Jan 1985–Dec 1990
Experiment:	Interannually varying surface forcing fields: (a) wind stresses within 30°N–30°S (blended with seasonal climatology poleward); (b) solar shortwave radiation

[Click on thumbnail for full-sized image.](#)

Table 2. Statistics of wind stress climatologies (10^{-2}N m^{-2}).

Station:	180°E	120°W	180°W	120°W	180°W
Mean of TAO zonal wind stress	-1.0	-3.6	-6.1	-5.0	-3.1
Mean of PSI zonal wind stress	-1.6	-3.6	-7.9	-6.8	-4.0
Mean of NCEP zonal stress	-1.6	-2.0	-5.2	-3.9	-2.4
Standard deviation of TAO-PSI	1.9	3.0	2.3	2.3	1.7
Standard deviation of TAO-NCEP	1.4	1.4	1.3	1.4	1.0
Standard deviation of PSI-NCEP	0.8	2.1	1.5	2.0	0.8
Standard deviation of TAO-NCEP	1.2	1.6	1.5	1.4	0.9

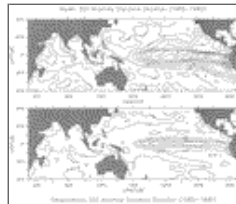
[Click on thumbnail for full-sized image.](#)

Figures



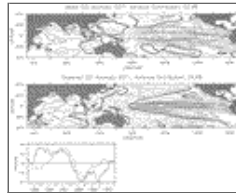
[Click on thumbnail for full-sized image.](#)

Fig. 1. Correlation between simulated SST anomalies and observed anomalies ([Reynolds and Smith 1994](#)) for 1985 to 1990. Shaded areas indicate negative values. Contour interval (C.I.): 0.2.



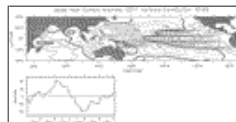
[Click on thumbnail for full-sized image.](#)

Fig. 2. Standard deviation of monthly SST anomalies for 1985 to 1990 (a) computed from the ocean model and (b) computed from observations ([Reynolds and Smith 1994](#)). C.I.: 0.2°C.



[Click on thumbnail for full-sized image.](#)

Fig. 3. First EOFs of SST anomalies for (a) model and (b) Reynolds SST data ([Reynolds and Smith 1994](#)). Shaded areas indicate negative values. C.I.: 0.1. (c) First EOF time series for the (solid) model and (dashed) observations. Multiplying the values in (a) and (b) with the corresponding values in (c) reproduces the original signal ($^{\circ}\text{C}$).



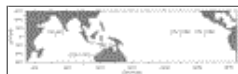
[Click on thumbnail for full-sized image.](#)

Fig. 4. (a) First EOFs of anomalies in upper-ocean heat content (wrt 450 m). Shaded areas indicate negative values. C.I.: 0.1. (b) EOF time series for first EOF. Multiplying the values in (a) and (b) reproduces the original signal ($^{\circ}\text{C m}$).



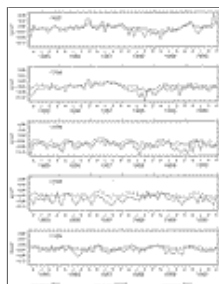
[Click on thumbnail for full-sized image.](#)

Fig. 5. Hovmoeller plots of (a) modeled and (b) observed (Reynolds and Smith 1994) SST anomalies along the equator for 1985 to 1990. C.I.: 1°C. The dashed lines at 66°E, 140°W, and 110°W indicate locations of XBT/buoy data chosen for comparison with model data.



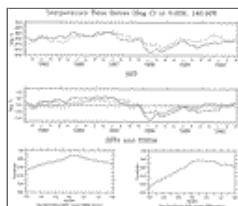
[Click on thumbnail for full-sized image.](#)

Fig. 6. Geographical positions of model time series, XBT data (Indian Ocean and Indonesian Throughflow), and TAO buoys (Pacific Ocean) used in this study.



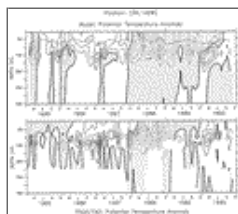
[Click on thumbnail for full-sized image.](#)

Fig. 7. (a) Time series of monthly mean wind stress climatologies along the equator at (a) 165°E, (b) 170°W, (c) 140°W, (d) 125°W, and (e) 110°W for 1985–90. Solid: FSU data (Legler et al. 1989; Stricherz et al. 1992), dashed: NCEP data (Kalnay et al. 1996), dotted: TAO data (Hayes et al. 1991). Units are newtons per square meter.



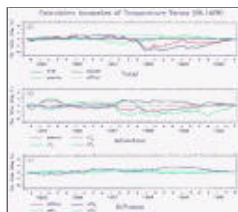
[Click on thumbnail for full-sized image.](#)

Fig. 8. (a) Time series of modeled (solid) and observed (Reynolds and Smith 1994; dashed) SST at 0°, 140°W for 1985–90. (b) Corresponding modeled (solid) and observed (dashed) SST anomaly plus averaged temperature anomaly of the model in the top 300 m, T300A (dotted). (c) Lead/lag correlation for modeled SST anomaly vs modeled T300A. (d) Lead/lag correlation for observed SST anomaly vs observed T300A. Positive (negative) values: T300A (SST anomaly) leads.



[Click on thumbnail for full-sized image.](#)

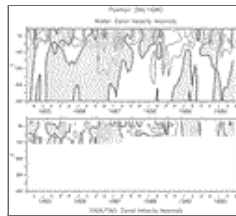
Fig. 9. (a) Time vs depth plots of potential temperature anomalies at 0°, 140°W for 1985–90 from (a) the model and (b) the TOGA/TAO array. C.I.: 1.0°C. The dashed line in (a) is the depth of the simulated mixed layer depth, as defined as the depth at which density was 0.5 kg m⁻³ higher than in the top level. Shaded areas indicate negative values.



[Click on thumbnail for full-sized image.](#)

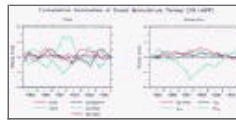
Fig. 10. Cumulative anomalies of potential temperature integrated over mixed layer depth at 0°, 140°W as a function of time: (a) time rate of change of temperature, net surface heat flux, total advection, and total diffusion; (b) horizontal advection plus individual contributions from zonal, meridional, and vertical advection; (c) horizontal diffusion plus individual contributions from zonal, meridional, and vertical diffusion. All terms are explained in the corresponding legends. Units are in °C. The mixed layer

depth has been defined as the depth at which density exceeds that at 7.5 m by 0.5 kg m^{-3} .



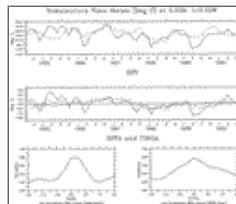
Click on thumbnail for full-sized image.

Fig. 11. (a) Time vs depth plots of zonal velocity anomalies at 0° , 140°W for 1985–90 from (a) the model and (b) the TOGA/TAO array. C.I.: 0.2 m s^{-1} . Shaded areas indicate negative values.



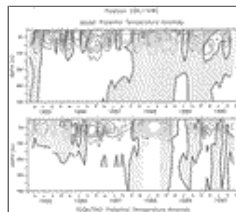
Click on thumbnail for full-sized image.

12. (a) Cumulative anomalies of zonal momentum integrated over mixed layer depth at 0° , 140°W as a function of time: (a) time rate of change of zonal velocity, zonal wind stress, total pressure gradient, total advection, and total friction. (b) Horizontal advection plus individual contributions from zonal, meridional, and vertical advection. All terms are explained in the corresponding legends. Units are in m s^{-1} . The mixed layer depth has been defined as the depth at which density exceeds that at 7.5 m by 0.5 kg m^{-3} .



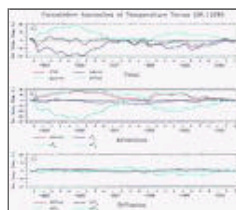
Click on thumbnail for full-sized image.

Fig. 13. Same as [Fig. 8](#) except at 0° , 110°W .



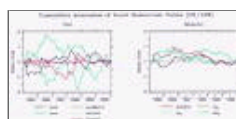
Click on thumbnail for full-sized image.

Fig. 14. Same as [Fig. 9](#) except at 0° , 110°W .



Click on thumbnail for full-sized image.

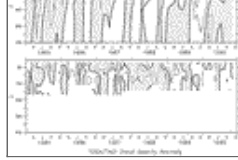
Fig. 15. Same as [Fig. 10](#) except at 0° , 110°W .



Click on thumbnail for full-sized image.

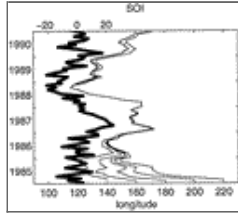
Fig. 16. Same as [Fig. 12](#) except at 0° , 110°W .





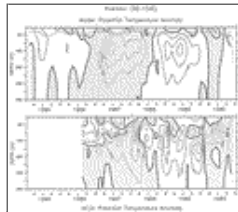
[Click on thumbnail for full-sized image.](#)

Fig. 17. Same as [Fig. 11](#) except at 0°, 110°W.



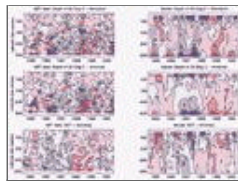
[Click on thumbnail for full-sized image.](#)

Fig. 18. Simulated trajectories of hypothetical drifters moved by 4°N–4°S averaged surface zonal currents. Initial points are at 140°E to 80°W with an interval of 20°. The SOI is superimposed as a thick line.



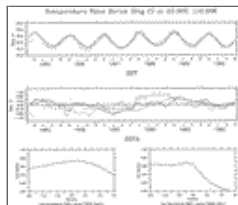
[Click on thumbnail for full-sized image.](#)

Fig. 19. (a) Time vs depth plots of potential temperature anomalies at 8°S, 124°E for 1985–90 from (a) the model and (b) XBT data. C.I.: 0.5°C. The dashed line in (a) is the depth of the simulated mixed-layer depth, which was defined as the depth at which density was 0.5 kg m^{-3} higher than in the top level. Shaded areas indicate negative values.



[Click on thumbnail for full-sized image.](#)

Fig. 20. Model to data comparison along XBT line IX1. (a, b) Variation in depth of the 20°C isotherm. The long-term mean depth in each observed (modeled) bin was subtracted from observed (modeled) values. (c, d) Anomaly in depth of the 20°C isotherm. The observed (modeled) mean annual cycle from 1985 through 1990 was subtracted from the observed (modeled) values. (e, f) Anomaly of SST. The mean observed (modeled) annual cycle for the period 1985 through 1990 was subtracted from the observed (modeled) values. The C.I. is 10 m (a–d) and 0.5°C (e and f).



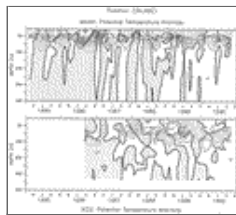
[Click on thumbnail for full-sized image.](#)

Fig. 21. (a) Time series of modeled (solid) and observed ([Reynolds and Smith 1994](#), dashed; XBT data, dotted) SST at 23°S, 112°E from 1985 to 1990. (b) Corresponding modeled (solid) and observed (dashed and dotted) SST anomalies plus averaged temperature anomaly in the top 450 m, T450A (dashed–dotted). (c) Lead/lag correlation for modeled SST anomaly vs modeled T450A. (d) Lead/lag correlation for observed SST anomaly vs observed T450A. Positive (negative) values: T450A (SST anomaly) leads.



Click on thumbnail for full-sized image.

Fig. 22. Same as [Fig. 18](#) except at 23°S, 112°E.



Click on thumbnail for full-sized image.

Fig. 23. Same as [Fig. 18](#) except at 0°, 66°E.

Corresponding author address: Dr. Andreas Schiller, CSIRO Division of Marine Research, GPO Box 1538, 7001 Hobart, Tasmania, Australia.

E-mail: schiller@marine.csiro.au

[top](#) ▲



© 2008 American Meteorological Society [Privacy Policy and Disclaimer](#)
Headquarters: 45 Beacon Street Boston, MA 02108-3693
DC Office: 1120 G Street, NW, Suite 800 Washington DC, 20005-3826
amsinfo@ametsoc.org Phone: 617-227-2425 Fax: 617-742-8718
[Allen Press, Inc.](#) assists in the online publication of *AMS* journals.